Mechanics & Industry **18**, 407 (2017)
© AFM, EDP Sciences 2017
DOI: 10.1051/meca/2017014

Mechanics & Industry

Available online at:
www.mechanics-industry.org

Regular Article

Effects of magnetic field on natural convection heat transfer in a T-shaped cavity

Adel Sahi[1,*], Djamel Sadaoui[1], Nacer Sadoun[2,3], and Abederrahmane Djerrada[1]

[1] Laboratoire de Mécanique, Matériaux et Energétique (L2ME), Faculté de Technologie, Université A. Mira de Bejaia, 06000 Bejaia, Algeria
[2] Laboratoire de Mécanique des Fluides Théorique et Appliquée (LMFTA), Faculté de Physique, Université des Sciences et de la Technologie Houari Boumediene (USTHB), 16111 Alger, Algeria
[3] Service Transferts, Interfaces et Procédés (TIPs), Faculté des Sciences Appliquées/Ecole Polytechnique, Université Libre de Bruxelles (ULB), CP165/67, avenue F.D. Roosevelt 50, 1050 Bruxelles, Belgium

Received: 11 April 2014 / Accepted: 20 February 2017

Abstract. This study was conducted to investigate the magnetic-field effect on the two-dimensional buoyancy-driven natural convection inside a grooved rectangular enclosure subjected to isothermal boundary conditions. The magnetohydrodynamic (MHD) equations, under Boussinesq approximation, are numerically solved using the finite volume method. Numerical simulations have been performed to investigate the free convective heat transfer induced by a temperature difference between the bottom hot wall and the upper cold flat wall. The numerical results, for wide range of Hartmann and Rayleigh numbers and for both horizontal and vertical magnetic field directions, are discussed in terms of velocity, temperature field, streamlines, isotherms, Nusselt numbers and reduction heat transfer ratio. The results highlighted the enclosure's performance condition and revealed that the heat and fluid flow fields are affected by the Rayleigh number and the magnetic field strength and direction. It is observed that increasing the Hartmann number damps the fluid flow, reduces the convection currents, decreases the average Nusselt number at the cold surface and has tendency to delay the transition to convection regime and lengthening the conduction zone. However, the use of magnetic field reduces heat exchange up to 30% with an optimal Rayleigh (Ra_{opt}) for each Hartmann number.

Keywords: thermal buoyancy / magnetic field / heat transfer reduction / natural convection / bifurcation

1 Introduction

Fluid flow and heat transfer inside different shaped enclosures are well-known natural phenomenon and have been the topic of many research engineering studies because of their applicability in various fields. The steady laminar free convection has been the subject of extensive theoretical and numerical investigations; the references [1–8], among others, gave some ideas about fluid flow and thermal characteristics inside cavities with different boundary conditions. Amongst the conclusions drawn from these investigations, it should be mentioned that the enclosure shape profoundly influences the free convection heat transfer. Others [9–16] have studied the influence of aspect ratio and have managed to emphasize the dependence of convective heat transfer with the space confined in the cavities.

Recently, research on heat transfer in industrial processes such as solar collectors, heat exchangers and nuclear reactor systems, has received great attention in order to cater for the growing needs for higher efficiencies. The influence of the magnetic field on the convective heat transfer and fluid flow are of paramount importance and particularly in some areas of renewable energy. Indeed, in solar engineering, a significant part of the incident energy on the thermal absorbers is exchanged (lost) by convection between the working fluid and the transparent top cover of the thermal solar collector. Several approaches are explored to minimize thermal loss and the MHD can be a promising technique in this field, a comprehensive literature survey concerned with this subject describes the usefulness of this technique. In earlier studies [17–22], attempts have been made to acquire a basic understanding of the flow and heat transfer characteristics in an enclosure in the presence of magnetic field. More recently, researches focus on the application of MHD as a control factor in the convection by damping both the flow and temperature oscillations in several energy conversion processes. In this

* e-mail: sahi.adel@hotmail.fr

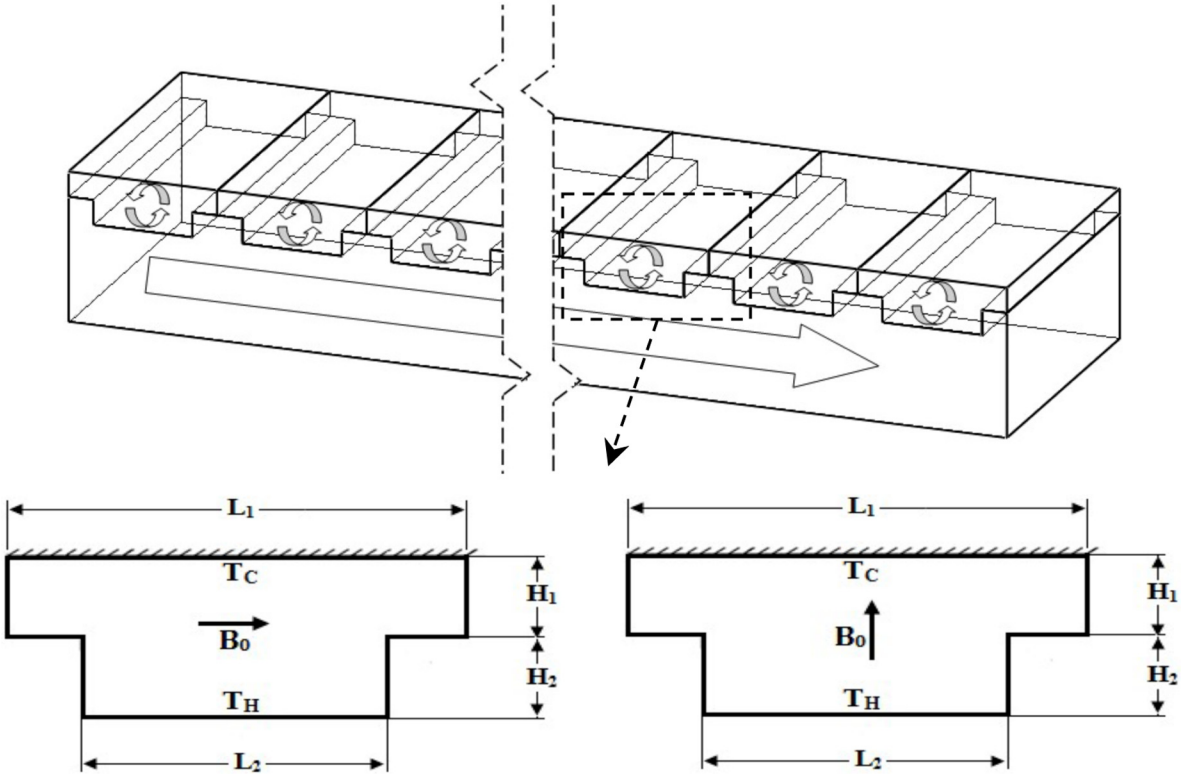

Fig. 1. Detail of cases studied.

perspective, the fluid experiences a Lorentz force and its effect is to alter the velocity and pressure characteristics of the flow which turn the affects in the heat transfer rate.

A literatures survey related to this topic are not as rich as without MHD, and revealed that most previous studies in this field are substantially orientated toward the study of natural convection inside cavities in the presence of a constant magnetic field. Different enclosure shapes including rectangular and cylindrical geometries subjected to various boundary conditions were considered by several authors [23–29]. The foregoing review revealed that the heat transfer rates and the flow field inside the enclosure depend strongly upon both the strength and direction of the magnetic field as well as the Rayleigh (Grashof) number. It was also observed that the flow oscillations were reduced or vanished for increased Hartmann numbers due to the magnetic field damping effect. On the other hand, the interaction with a magnetic field can delay the onset of natural convection currents and alter the heat transfer characteristics and fluid drag by reducing the fluid velocity. In addition, the results show a difference between the solutions of the full MHD equations and low-magnetic Reynolds approximation. Furthermore, natural convection flows in the presence of a magnetic field in a tilted enclosure for different thermal boundary conditions has also been investigated numerically until recently. In this regard, it is worth to outline that the enclosure inclination has importance on its performance [30–35] due to the change in the total net acceleration of gravitational and magnetizing forces. It can also be concluded that suppression effect of the magnetic field on convection currents and heat transfer is more significant for low inclination angles and high Grashof numbers. Finally, it should further be stated that magnetic field effect on flow driven by the combined mechanism of buoyancy and surface tension coupled to double-diffusive natural convection in view of the numerous potential applications has received considerable attention. Reviews on this subject can be found in the publications of Rudraiah et al. [36], Chamkha and Al-Naser [37], Changfeng [38], Sathiyamoorthy and Chamkha [39], Venkatachalappa et al. [40], Mansour and Bakier [41], Hussein et al. [42], Sheremet et al. [43] and Bondareva and Sheremet [44]. They namely reveal how the heat flux and the fluid flow organization depend on the magnetic field, so that an oscillatory motion of the flow that fades with the application of magnetic field and convection heat transfer is enhanced by thermocapillary force when buoyancy force is weakened.

The present paper will focus on the numerical steady laminar free convection inside a complex shaped enclosure with isothermal boundary conditions in presence of constant magnetic field. Despite the above circumstances, up to date, this geometrical enclosure shape, usually en countered in thermal solar collectors and considered by Chen and Cheng [45], has not been studied with MHD effect. The effects of pertinent parameters such as Rayleigh number, Hartmann number and magnetic field direction on buoyancy induced flow developments are considered. Special attention will be paid to the analysis of the bifurcation to convection regime. The results obtained are compared with the available references and presented in terms of streamlines, isotherms and Nusselt numbers.

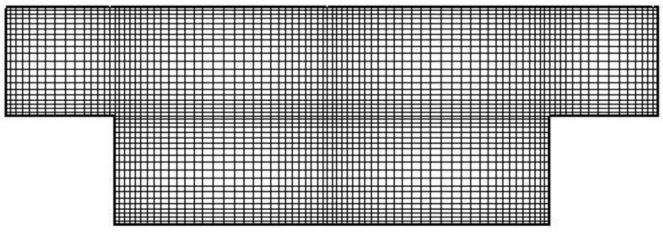

Fig. 2. Detail of the computational grid within the partitioned enclosure.

Correlation for Ra_c corresponding to the transition to convection regime is presented as a function of Hartmann number.

2 Mathematical formulation

The schematics of both considered physical models are sketched in Figure 1. The two-dimensional shallow cavity under consideration consists of two surfaces with grooved part on the bottom, such as the upper wall is maintained at a cold temperature (T_C), and the others sides are at fixed warm temperature (T_H).

In Figure 1, H_1, L_1 and H_2, L_2 shows the height and the width of the enclosure and the microcavity, respectively. For simplicity, the geometric ratios are defined such as: $a = L_1/L_2 = 1.5$, $b = H_1/H_2 = 1$ and $c = H_1/L_2 = 1/4$. However, gravitational force acts in vertical direction and a magnetic field of strength B_o is applied horizontally ($\phi = 0$) or vertically ($\phi = \pi/2$) normal to the side walls.

The set of magnetohydrodynamic and heat transfer equations for Newtonian fluid flow includes the Navier-Stokes equations of motion, the equation of mass continuity and the energy equation. Low magnetic Reynolds number for the MHD flow cases is invoked so that the induced magnetic field in the medium is also neglected compared to the applied magnetic field. The fluid properties are also assumed to be constant, except for the density in the buoyancy term to relate the density changes to temperature, which follows the Boussinesq approximation. In differential form, under some assumptions as neglected effects of viscous dissipation, Joule heating, Hall effect, compressibility and radiation the quasi-steady fluid mechanics equations are cast in their dimensionless form as follows:

$$\frac{\partial V_i}{\partial X_i} = 0 \tag{1}$$

$$V_j \frac{\partial V_i}{\partial X_j} = -\frac{\partial p}{\partial X_j} + \frac{\partial^2 V_i}{\partial X_j \partial X_j} + \frac{Ra}{Pr}\theta\delta_{i2} - Ha^2 V_\perp \tag{2}$$

$$V_j \frac{\partial \theta}{\partial X_j} = \frac{1}{Pr}\frac{\partial^2 \theta}{\partial X_j \partial X_j} \tag{3}$$

F_i are the total body forces at X_i directions and they are defined as follows:

$$F_1 = Ha^2(V \sin\phi \cos\phi - U \sin^2\phi) \tag{4}$$

$$F_2 = \frac{Ra}{Pr}\theta + Ha^2(U \sin\phi \cos\phi - V \cos^2\phi) \tag{5}$$

where ϕ is the magnetic field direction while Ra, Pr, Ha are the Rayleigh, Prandtl and Hartmann number, respectively. Ra gives a measure of the relative importance of buoyancy to viscous, Pr represents the ratio of viscous to thermal diffusivities and Ha is an average measure of the ratio of magnetic to viscous forces. In the above equations, P, θ, X_i and V_i are the dimensionless pressure and temperature, the dimensionless Cartesians coordinates and corresponding velocity components respectively. In the equation of motion, the sign of Ha is opposite to the sign of Ra, so that there is an opposite effect of Ra and Ha on flow regime and Nusselt number.

Assuming the non-slip flow, the dimensionless boundary conditions are established with prescribed temperature $\theta = 0$ and $\theta = 1$ at the top wall and on the other sides, respectively. The relevant boundary conditions can be written as follows:

$$V_i = 0, \quad \theta = 0 \quad \text{(Upper wall)} \tag{6}$$

$$V_i = 0,$$
$$\theta = 1 \quad \text{(Vertical and grooved bottom walls)} \tag{7}$$

The local and average Nusselt numbers at the upper cold wall are given by:

$$Nu_X = \frac{\partial \theta}{\partial X}, \quad \overline{Nu} = \int_{-(1/2)}^{1/2} Nu_X \, \mathrm{d}X, \quad \text{respectively.} \tag{8}$$

3 Numerical procedure

The non-dimensional governing equations (Eqs. (1)–(3)) along with the boundary conditions (Eqs. (4) and (5)) are solved numerically by the finite volume method using Patankar's SIMPLE algorithm [46]. The advective terms are discretized by a QUICK scheme whereas a second-order central difference scheme is applied for the diffusion terms (for more details, see [46]). The convergence criterion is to reduce the maximum residual of the grid control volume below smaller than 10^{-9}. A non-uniform grid spacing is used to discretize the domain and a grid testing is performed with various grid combination (21×21 to 201×201) with small elements near the walls where the most important gradients are located (Fig. 2). Table 1 presents a comparison of the predicted average Nusselt-numbers using different grid arrangements.

Table 1. Effects of the grid size on the mean Nusselt number. Comparison between present work and that of Chen and Cheng [45].

Gr	Grid	Nu		Deviation (%)
		Present	[45]	
10^4	41 × 41	9.467	–	–
	81 × 81	10.665	–	–
	121 × 121	11.034	–	–
	161 × 161	11.056	11.132	0.683
	181 × 181	11.059	11.132	0.653
	201 × 201	11.620	11.132	0.629
5×10^4	161 × 161	13.943	13.914	0.208
10^5		15.493	15.582	0.371
2×10^5		17.587	17.704	1.463

Table 2. Effects of the grid size on the maximum stream function and the mean Nusselt number. Comparison between the current work and that of Sarris et al. [47].

Gr	Ha	Grid	Ψ_{max}		Deviation (%)	Nu		Deviation (%)
			Present	[47]		Present	[47]	
10^4	0	41 × 41	6.119	–	–	1.978	–	–
		81 × 81	6.136	–	–	1.991	–	–
		121 × 121	6.137	–	–	1.997	–	–
		161 × 161	6.137	–	–	2.000	2.020	1.000
	25	161 × 161	1.661	1.664	0.180	1.160	1.161	0.086
10^6	0	161 × 161	21.737	21.895	0.722	7.999	7.976	0.288
	100		7.197	7.230	0.456	3.197	3.183	0.440

Results show that the values remain almost the same for grids finer than 121 × 121 and heavily depend on the grid size for less fine grids. Nevertheless, similar tests were conducted for others Rayleigh numbers and the grid size were adjusted accordingly. Extensive validations of the developed code for MHD in concave square enclosure have been also validated against the results reported by Sarris et al. [47]. The computations have been performed in terms of mean Nusselt number, maximum stream function, streamline and isotherm patterns for various Rayleigh numbers (10^3 and 10^6).

As shown in Tables 1 and 2 and Figure 3, the comparisons are in excellent agreements, providing sufficient confidence in present computations. Consequently, considering both the accuracy and the computational costs, most computations reported in the current work were performed with a multiple grid system of 161 × 161.

Furthermore, extensive validations of the developed code for natural convection in an air-filled square cavity crossed with a magnetic field were also done. The mean Nusselt number numerically deduced are compared to those obtained by Sarris et al. [47] for various Grashof and Hartman numbers. As listed in Table 2; the comparisons are in good agreements with the benchmark cases.

4 Results and discussion

Different scenarios for magneto-convection in a partitioned enclosure were explored for Rayleigh and Hartmann numbers ranging from 10^3 to 10^6 and from 0 to 105, respectively, for different magnetic field direction. In order to discuss the effects of both Ra and Ha only, the other parameters are kept as constant $Pr = 0.71$, aspect ratio $a = 3/2$, $b = 1$ and $c = 1/4$.

4.1 Temperature and fluid pattern (streamlines and isotherms)

Figures 4 and 5 depict the effect of both Rayleigh and Hartmann numbers on the flow pattern and temperature distribution in the concave enclosure for horizontal and vertical magnetic field.

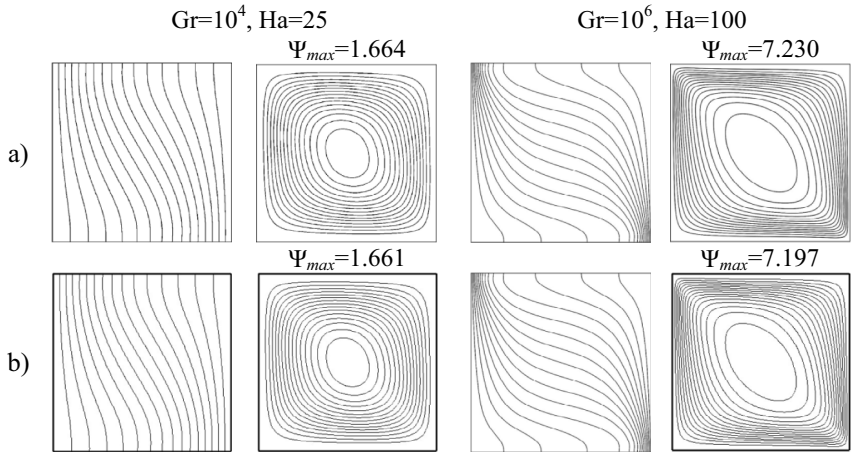

Fig. 3. Comparison of isotherms and streamlines. (a) Sarris et al. [47] and (b) present study.

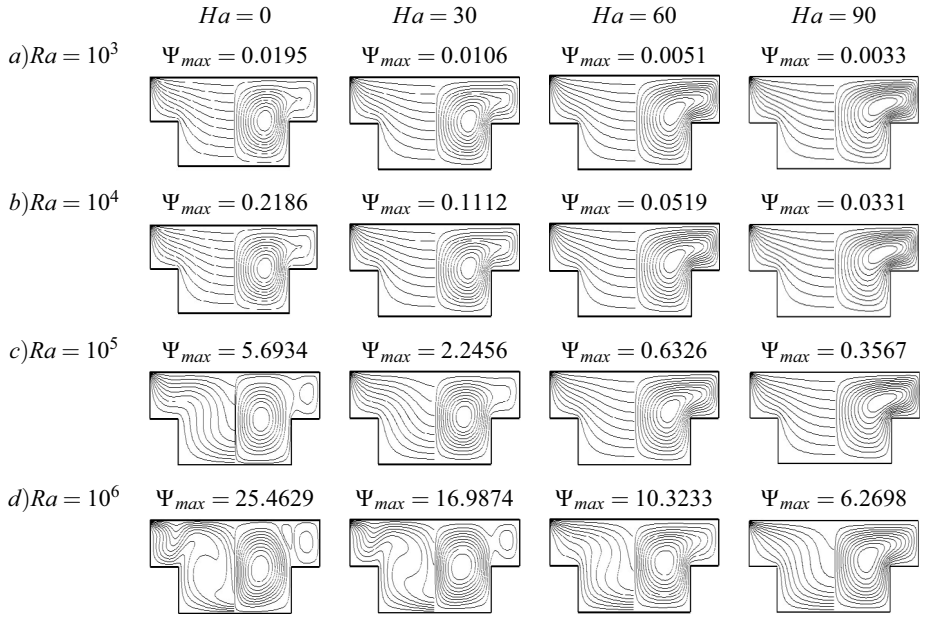

Fig. 4. Isotherms (left) and streamlines (right) for horizontal magnetic field direction ($\phi = 0$).

In the absence of the magnetic field ($Ha = 0$), both Figures 4a and 5a are similar, heated fluid rises above the heater and they impinged each other at the middle of the enclosure showing a bi-cellular than a multi-cellular behavior within the micro-cavity. For small values of Rayleigh number ($\leq 10^4$), the fluid motion involves two primaries and symmetric recirculating eddies of relatively weak velocity extending throughout the partitioned cavity with clockwise and anti-clockwise rotations ($\Psi_{\max} = \Psi_{\min} \leq 0.2186$). The isotherm plots are smooth curves which cover the entire enclosure and present a symmetric behavior about the vertical axis indicating that the conduction is the dominant heat transfer mechanism. The isotherms values change smoothly from the hot to the cold wall with decreasing from the bottom to the top along the vertical centerline of the cavity.

Increasing Rayleigh number ($Ra > 10^4$), due to the important temperature gradient generates the faster recirculation rolls ($0.2186 < \Psi_{\max} \leq 25.4929$). Minor cells appear near the upper corners of the cavity with negligible intensity when compared with the main circulation cells.

The temperature contours change significantly so that isothermal plumes appear and turn back towards the hot wall without disturbing the vertical symmetry. It is clearly observed that the buoyancy strength induces the increasing vortices for $10^4 < Ra \leq 10^6$, this is owing to the dominating

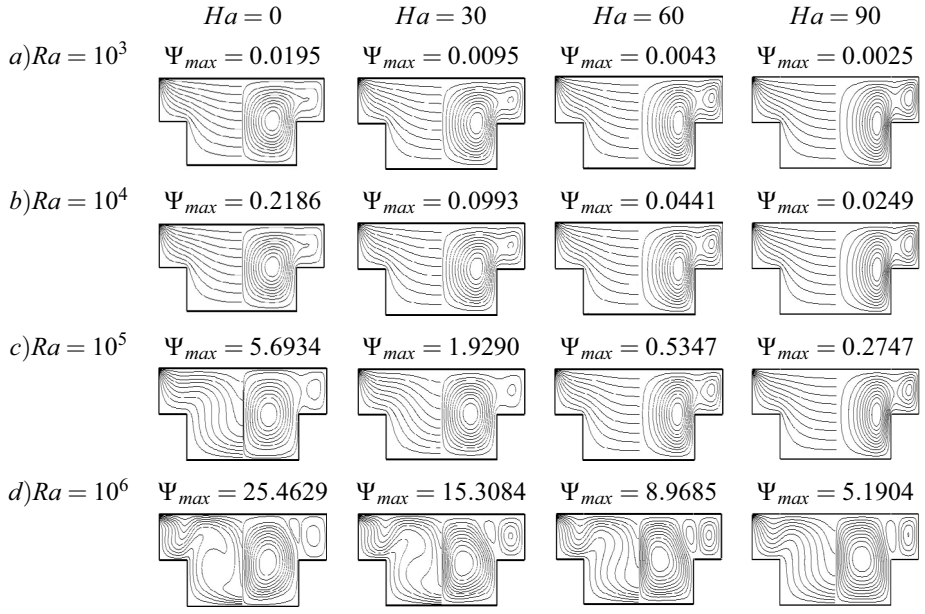

Fig. 5. Isotherms (left) and streamlines (right) for horizontal magnetic field direction ($\phi = \pi/2$).

Table 3. Maximal stream function ($\Psi_{\max}$) for horizontal ($\phi = 0$) and vertical ($\phi = \pi/2$) magnetic field direction.

Ra	$Ha = 0$		$Ha = 30$		$Ha = 60$		$Ha = 90$	
	$\phi = 0$	$\phi = \pi/2$	$\phi = 0$	$\phi = \pi/2$	$\phi = 0$	$\phi = \pi/2$	$\phi = 0$	$\phi = \pi/2$
10^3	0.0195	0.0195	0.0106	0.0095	0.0051	0.0043	0.0033	0.0025
10^4	0.2186	0.2186	0.1112	0.0993	0.0519	0.0441	0.0331	0.0249
10^5	5.6934	5.6934	2.2456	1.9290	0.6326	0.5347	0.3567	0.2747
10^6	25.4929	25.4929	16.9874	15.3084	10.3233	8.9685	6.2698	5.1904

influence of the convective current in the cavity. Thus, increasing (Ra) promotes the convection heat transfer mechanism against conduction.

In the presence of a magnetic field ($Ha \neq 0$), Figures 4 and 5 show that increasing its intensity by increasing the Hartmann number, leads to decreases the strength of circulations. For a horizontal magnetic field direction as seen from Figure 4b–d, the streamlines are crowded near the upper sides of the cavity and the core of the vortex shifted towards the top corners then tends to be stretched in the horizontal direction. The strength of main flow is decreased with increasing Ha indicating that the magnetic field is becoming more effective on main flow. Since, the application of a transverse magnetic field has the tendency to slow down the movement of the fluid in the enclosure.

For $Ra > 10^4$, separated slower recirculating eddies positioned close to each top vertical sides becomes shorter and merged into two single ones and becomes comparatively large extending throughout the enclosure. As a result, the strength of these circulations increases as the Rayleigh number increases and decreases as the Hartmann number increases (e.g. for $Ra = 10^5$: $\Psi_{\max} = 5.6934$ for $Ha = 0$ and $\Psi_{\max} = 0.3567$ for $Ha = 90$; for $Ra = 10^6$: $\Psi_{\max} = 25.4929$ for $Ha = 0$ and $\Psi_{\max} = 6.2698$ for $Ha = 90$).

Furthermore, the isotherms are affected by the presence of magnetic field so that the thermal boundary layer at the two active side walls vanishes and the isothermal distortion are straighten out gradually to take the shape of horizontal lines in the core of the micro-cavity without disturbing the vertical symmetry.

This is an indication of weaker convection flows at higher Ha. For $Ra < 10^6$, velocity and temperature contours indicate that the heat transfer will be of almost conductive type beyond $Ha = 60$. In other words, results explain that an increase either in Ra or in Ha affect both the flow behavior and heat transfer characteristics inside the enclosure.

The impacts due to change in magnetic field strength and direction are depicted in Figure 5b–d where an increase in the Hartmann number results in the isotherms changing from distorted behavior to horizontal distribution in the core region. Moreover, as summarized in Table 3, among the cases studied, the effect of vertical magnetic field is more noticeable than that of horizontal direction and makes more effect on the natural convection. Further, as seen in Figures 4 and 5, at high Rayleigh numbers ($Ra = 10^6$) the convection regime prevails in the enclosure for $Ha \geq 90$. Whatever (regardless) the magnetic field direction while for low Rayleigh values the convective mode heat transfer is converted into conductive one.

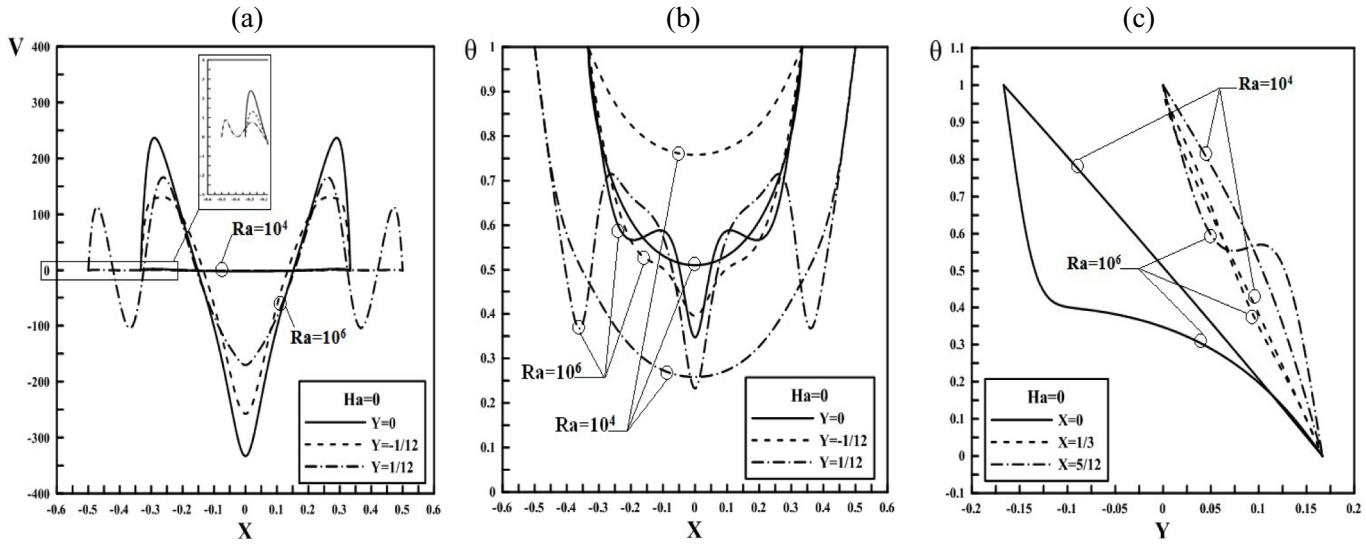

Fig. 6. V-velocity and temperature profiles in the cavity for $Ha = 0$.

4.2 Velocity and temperature profiles

Dimensionless vertical velocity (V) and temperature distribution (θ) along horizontal axis x (vertical axis y) are presented respectively in Figure 6a–c for three positions located at $x = 0, 1/3$ and $5/12$ ($y = -1/2, 0, 1/2$). In absence of magnetic field ($Ha = 0$) it is evident that the velocity and temperature profile are symmetric with respect the vertical centerline. As already pointed out in the streamlines analysis, the fluid in the core region ($-0.333 \leq x \leq 0.333$) is driven by an upward movement (from bottom to the top cavity) in the vicinity of the hot vertical walls.

Getting at the cold wall, the fluid flow becomes horizontal and falls down towards the vertical centerline. Besides, the maximum V-velocity are located in the vicinity of the vertical hot walls and near the top cavity ($y = 1/2$) on the extension of the microcavity's verticals sides at the contact between the upward and downward flow. The results show that at low Rayleigh number, the velocity profile does not significantly varying along the horizontal section indicating a weak circulation zone, therefore the heat transfer by conduction is dominant. Further increases in the Rayleigh number enhance the velocity values, so that the maximum V-velocity increases due to the strong buoyant flows. The contact between primary cells correspond to a minimum velocity value, the contribution of co-rotating cells is cumulated. This influence can also be inferred from the temperature profiles. The temperature distribution shows that below $Ra = 10^4$ temperatures are smooth. Beyond, this behavior is modified and the convection becomes gradually dominant.

As moving from bottom to the top ($y = -1/2$, 0, $1/2$), the temperature grows considerably. For a fixed position (y), the fluid is heated in the surrounding area of the vertical sides, and cooled when moving towards the core region. Figure 7a and b display the effects of magnetic field strength ($Ha = 0$ to 105) on velocity components and temperature profiles on vertical centerline and at the opening ($y = 0$). It is showed that both the velocity and temperature fields are characterized by sharp drops in their values near the vertical sides due to the boundary layer effect. As can be noticed increasing Ha leads to decrease the maximum V-velocity and deceleration of the fluid due to the influence of the magnetic field on the convective flows. Moreover, the Hartmann number has an insignificant influence on the temperature profile at $Ra = 10^4$, the thermal field is similar to that of pure thermal convection in the absence of magnetic field. Here the heat transfer is mainly due to conduction. For $Ra = 10^6$, when the convection flows occur, the influence of Ha is strong and the temperature distortions are significantly disturbed. We can conclude that due to the flow damping effect of the Lorentz force, the magnetic field strength reduces considerably the flow velocity hence the rates of heat transfer especially for large values of Ha. By applying magnetic field both cases are damped similarly, Figure 7b and c so that velocity profiles are flattened and temperature profiles are smooth for higher values of the Hartmann.

4.3 Nusselt number

Figure 8a displays the distribution of the local Nusselt number (Nu_x) along the cold wall of the enclosure at various Rayleigh numbers ($Ra = 10^3$–10^6) in absence of magnetic field ($Ha = 0$). While Figure 8b and c depict the effect of Hartmann number on the local Nusselt number (Nu_x) on the same wall for $Ra = 10^6$, following two magnetic field directions.

The results presented in Figure 8a show that, for all Rayleigh numbers, the local Nusselt profiles are symmetric with respect to the vertical axis ($x = 0$). The peaks observed correspond to the tightening of the thermal boundary layer along the cold wall. The minimum heat transfer rate, resulting from the relaxation of the thermal boundary layer occurs at the middle wall as seen from streamlines and isotherms contours (Figs. 4 and 5). As a result of increasing Ha (Fig. 8b–c), the rate of heat transfer along this wall decreases but at different scales according to the magnetic field strength and direction so that curves becomes gradually smooth and tends to those of the conduction regime ($Ra \leq 10^4$).

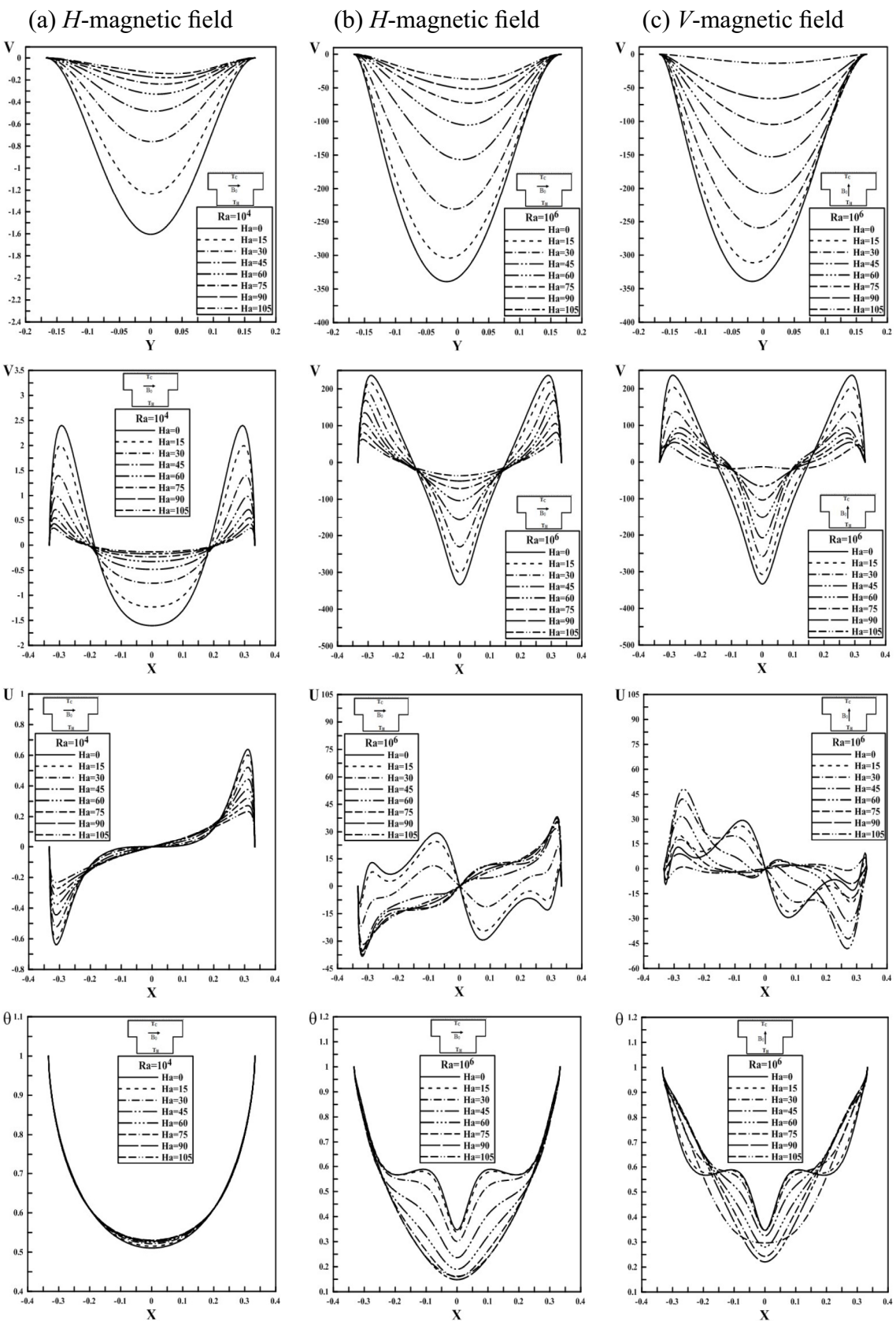

Fig. 7. Effect of magnetic field strength and direction on velocity component and temperature profiles.

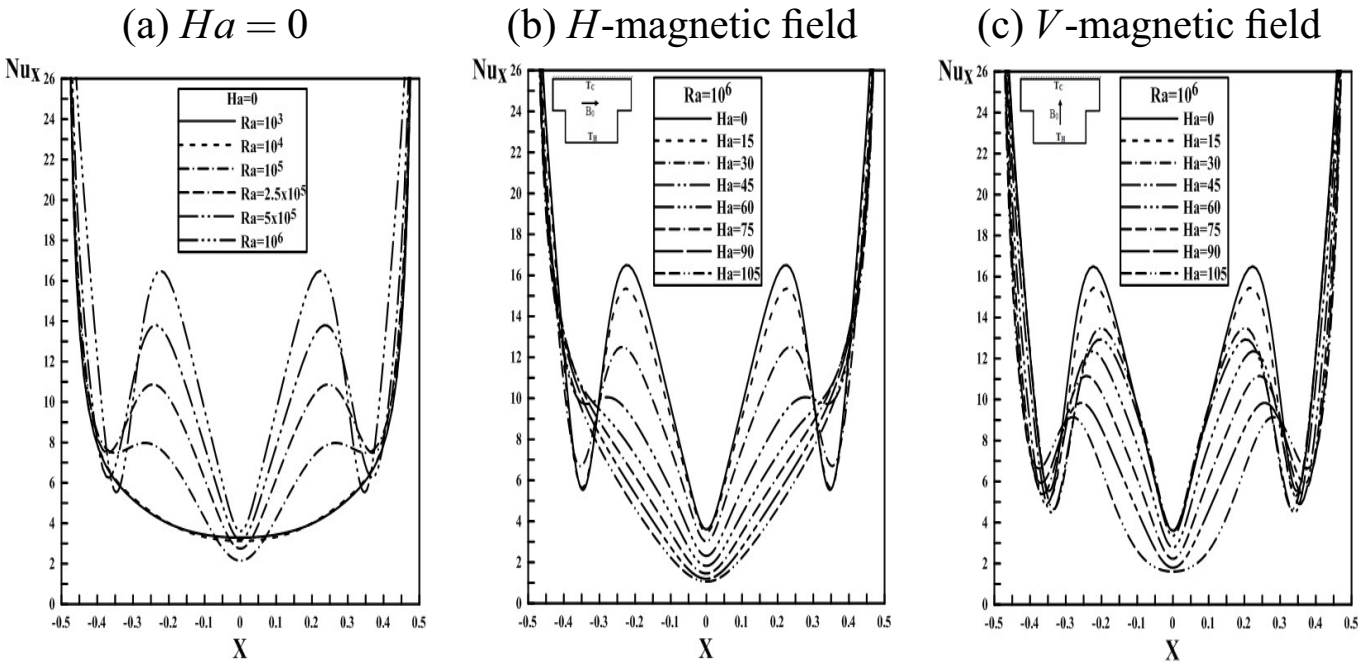

Fig. 8. Local Nusselt on the upper cold wall.

Table 4. Effect of magnetic field strength and direction on mean Nusselt number.

Ha	Ra					
	H-magnetic field, $\phi = 0$			V-magnetic field, $\phi = \pi/2$		
	10^4	10^5	10^6	10^4	10^5	10^6
0	10.639	12.060	16.893	10.639	10.060	16.893
15	10.638	11.672	16.381	10.637	11.658	16.515
30	10.636	10.972	15.139	10.636	10.910	15.814
45	10.636	10.712	14.304	10.636	10.685	15.167
60	10.636	10.664	13.755	10.636	10.653	14.477
75	10.636	10.650	13.186	10.636	10.644	13.559
90	10.636	10.644	12.613	10.636	10.640	12.666
105	10.636	10.641	12.075	10.636	10.638	11.822

The variation of the average Nusselt number, deduced from the integration of the local Nusselt number distribution, is used to evaluate the overall heat transfer rate and is investigated for different values of Rayleigh and Hartmann numbers as illustrated in Table 4 and Figures 9–11. To focus the effect of magnetic field on the heat transfer at the upper wall, Figure 9a and b show the variation of mean Nusselt number with the Hartmann number at different values of the Rayleigh number. When the heat transfer is only due to conduction ($Ra = 10^3$ to 10^4) the magnetic field does not entail any significant change in heat transfer and the mean Nusselt number remains unchanged whether increasing Hartmann or Rayleigh numbers. Also, it is noticed that heat transfer depends strongly on magnetic field strength for higher Rayleigh number, where the heat transfer is partly or mainly due to convection. The increase in the Hartmann number damps the flow field and greatly weakens the convection currents, leading to reduce the value of Nusselt number.

The dependence of the mean Nusselt number on Rayleigh number is displayed in Figure 10a and b for horizontal and vertical magnetic field direction respectively. It is observed that due to the strengthened buoyant flow, the mean Nusselt number increases as the Rayleigh number increases. Magnetic field strength has a more noticeable effect on heat transfer at higher Rayleigh number here the buoyant flows are significantly influenced by Ha, so that the overall heat transfer decreases as summarized in Table 4. This delays the transition from conductif regime to the convectif one. However, the presence of magnetic field has tendency to delay this transition and lengthening the conduction zone.

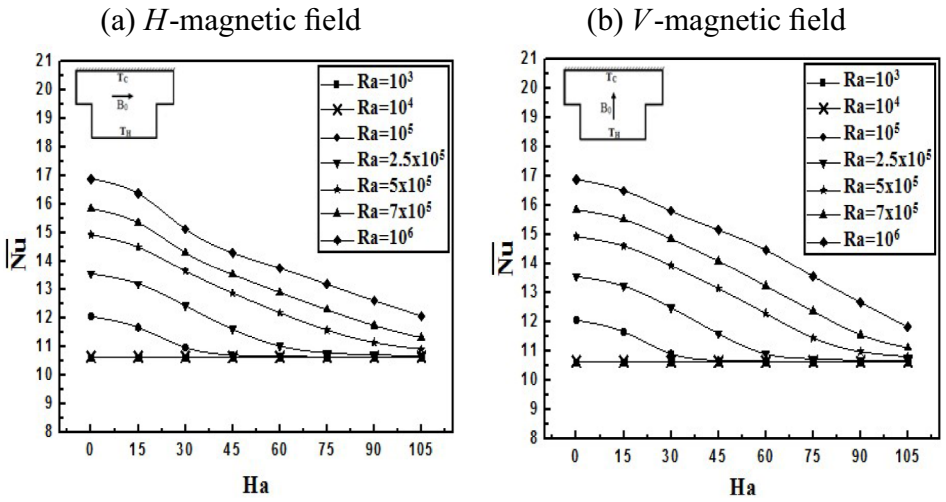

Fig. 9. Average Nusselt number versus Hartmann for different Rayleigh numbers. H-magnetic field on the left and V-magnetic field on the right.

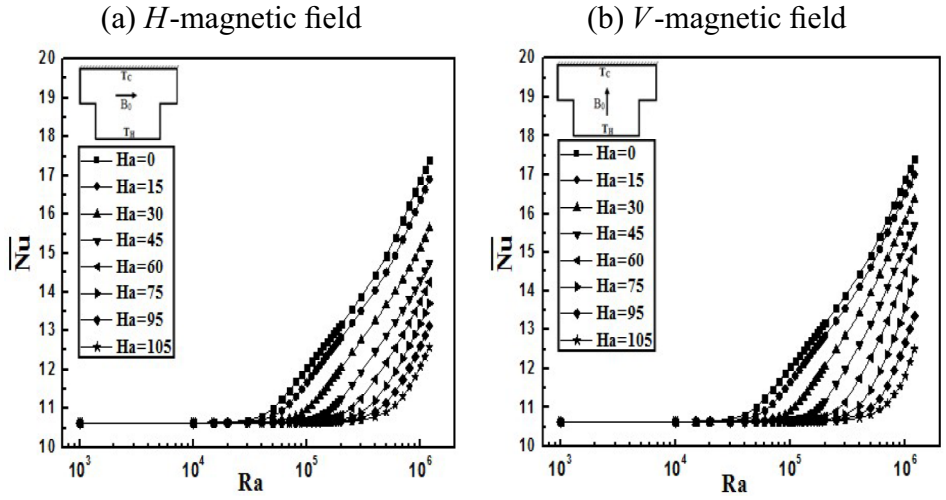

Fig. 10. Average Nusselt versus Rayleigh for different Hartmann numbers. H-magnetic field on the left and V-magnetic field on the right.

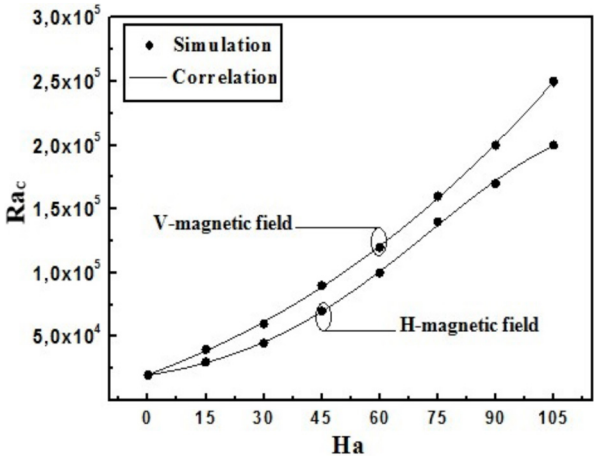

Fig. 11. Comparison between simulation and correlation proposed for critical Rayleigh number, Ra_c.

Figure 11 and Table 5 give the values of critical Rayleigh (Ra_c) corresponding to bifurcation to the convective regime for different value of Ha; which clearly shows that increasing magnetic field strength, leads to an increase of the value of the critical Rayleigh number Ra_c, thus extending the conduction zone. Moreover, Ra_c for the two configurations can be correlated pretty well with the Hartmann number for a maximum deviation less than 2%, as follows:

$$Ra_c = C_1 + C_2 \exp\left(-\frac{(Ha - C_3)^2}{2C_4^2}\right) \tag{9}$$

where the coefficients C_1, C_2, C_3 and C_4 are given as follows:

Table 5. Critical and optimal Rayleigh number for different Ha (deviation between simulation and correlation).

Ha	V-magnetic field, $\phi = \pi/2$				H-magnetic field, $\phi = 0$			
	$10^{-5} \times Ra_{opt}$	$10^{-5} \times Ra_c$		Deviation (%)	$10^{-5} \times Ra_{opt}$	$10^{-5} \times Ra_c$		Deviation (%)
		Simulation	Correlation			Simulation	Correlation	
0	–	0.200	2.018	1.90	–	0.200	0.199	0.588
15	0.800	0.400	0.389	2.659	0.900	0.300	0.296	1.238
30	1.200	0.600	0.617	2.772	1.000	0.450	0.458	1.729
45	1.800	0.900	0.889	2.249	1.100	0.700	0.697	0.416
60	3.000	1.200	1.210	0.836	3.000	1.000	1.011	1.146
75	4.000	1.600	1.584	1.007	6.000	1.400	1.372	1.988
90	6.000	2.000	2.012	0.627	7.000	1.700	1.723	1.365
105	9.000	2.500	2.497	0.134	8.000	2.000	1.993	0.341

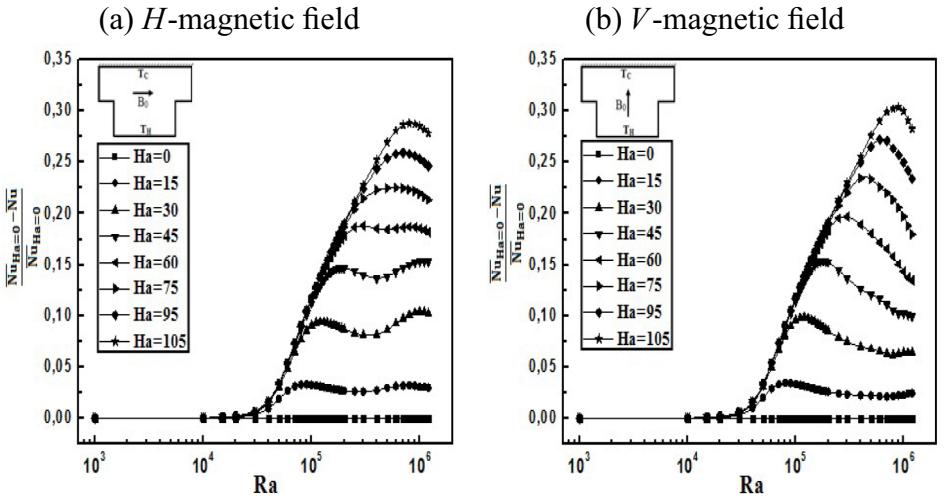

Fig. 12. Variation of average Nusselt ratio with Rayleigh number.

For H-magnetic field, $\phi = 0$

$$C_1 = 10146.72393,\ C_2 = 202085.45661,$$

$$C_3 = 123.17627,\ C_4 = 50.01299$$

For V-magnetic field, $\phi = \pi/2$

$$C_1 = -46400.53331,\ C_2 = 1.08267 \times 10^6,$$

$$C_3 = 330.11822,\ C_4 = 139.79525$$

These earlier observations are noted by the heat transfer reduction factor E in the enclosure. The reduction ratio due to the presence of magnetic field as a function of Rayleigh number is exhibited for various values of Hartmann number in Figure 12a and b through the ratio:

$$E = \frac{\overline{Nu}_{Ha=0} - \overline{Nu}}{\overline{Nu}_{Ha=0}} \tag{10}$$

It reveals the improvement of the performance of the enclosure with reducing heat loss through the cold wall. As pointed, the magnetic field strength gets no remarkable changes on enclosure performance for lower values of Ra where the conduction regime dominates. For higher Rayleigh ($Ra \geq 3 \times 10^4$) when the heat convection transfer is strong the ratio firstly increases sharply with increasing Rayleigh and then remains relatively constant so that curves appear flattened for intermediate Hartmann ($Ha \leq 60$ for H-magnetic field). While for highest Hartmann numbers ($Ha > 60$) the Nusselt reduction goes down rapidly and this corresponds to convection dominated region. These figures show that there is an optimal value Ra_{opt} for which the reduction ratio (E) is maximal. Both Ra_{opt} and $E_{\max}$ increases as the strength of magnetic field increases as summarized in Table 5.

The use of magnetic field allows us a reduction of heat loss by up to 30% for $Ha = 105$. However, this heat gain is not guaranteed for large Rayleigh numbers ($Ra > Ra_{opt}$). For this, it is preferable to use a horizontal magnetic field case with a strength corresponding to $Ha = 60$ allowing a stable thermal gain around 20% even for high Rayleigh numbers.

5 Conclusion

Natural convection heat transfer inside complex enclosure's wall in the presence of a magnetic field has been carried out with $Pr = 0.71$. The effects of several parameters such as the Rayleigh number, the Hartmann number and magnetic field direction on the flow and thermal behavior have been examined. Numerical results for the steady state in term of streamlines and temperature contours within the grooved concave enclosure have been reported and led to the following conclusions:

- the magnetic field does not alter the symmetry of results (streamlines, isotherms and local Nusselt number);
- the magnetic field reduces the convection currents and promotes the heat transfer by conduction whatever its orientation;
- increasing Hartmann number damps the fluid flow and has tendency to delay the transition (bifurcation) to convection regime and lengthening the conduction zone. A correlation has been proposed for Ra_c as function of Hartman number;
- for both cases (H- and V-magnetic field) reduction heat transfer ratio (E) shows that there is an optimal Rayleigh (Ra_{opt}) for each Hartmann number;
- the use of magnetic field allows us a reduction of heat losses approaching 30% for $Ha = 105$, this thermal gain goes down rapidly for highest Rayleigh in both cases (H- and V-magnetic field direction). So that it is preferable to use a horizontal magnetic field case with a strength corresponding to $Ha = 60$ allowing a stable thermal gain around 20% even for high Rayleigh numbers.

Nomenclature

a,b,c	enclosure aspect ratio ($a = L_1/L_2$; $b = H_1/H_2$; $c = H_1/L_2$)
C_p	specific heat at constant pressure ($\mathrm{J\,kg^{-1}\,K^{-1}}$)
g	gravitational acceleration ($\mathrm{m\,s^{-2}}$)
Gr	Grashof number, $Gr = Ra/Pr$
H	height (m)
L	length (m)
k	thermal conductivity ($\mathrm{W\,m^{-1}\,K^{-1}}$)
B_0	magnitude of magnetic field ($T = \mathrm{kg\,s^{-2}\,A^{-1}}$)
$\underline{Nu_x}$	local Nusselt number
$\overline{Nu}$	average Nusselt number
$p(P)$	dimensional (dimensionless $P = p \times L^2/(\rho \times \nu^2)$) pressure (Pa)
Pr	Prandtl number, $Pr = \nu/\alpha$
Ra	Rayleigh number, $Ra = g \times \beta \times (T_H - T_C) \times L^3/(\alpha \times \nu)$
Ha	Hartmann number, $Ha = B_o L(\sigma/\mu)^{1/2}$
T	temperature (K)
$v_i(V_i)$	dimensional (dimensionless $V_i = \mathrm{v_i L}/\nu$) velocity components ($\mathrm{m\,s^{-1}}$)
$x_i(X_i)$	dimensional (dimensionless $X_i = x_i/L$) Cartesian coordinates (m)

Greek symbol

ρ	density ($\mathrm{kg\,m^{-3}}$)
α	thermal diffusivity ($\mathrm{m^2\,s^{-1}}$)
β	thermal expansion coefficient ($\mathrm{K^{-1}}$)
μ	dynamic viscosity ($\mathrm{kg\,s^{-1}\,m^{-1}}$)
ν	kinematic viscosity ($\mathrm{m^2\,s^{-1}}$)
σ	electric conductivity ($\mathrm{m\,s^3\,A^2\,kg^{-1}}$)
θ	dimensionless temperatures, $\theta = (T - T_C)/(T_H - T_C)$
Ψ	dimensionless stream function, $\Psi = \psi/\nu$
δ_{ij}	Kronecker delta

Subscripts

H, C	hot and cold
1, 2	enclosure and micro-cavity

References

[1] M.S. Khelifi-Touhami, A. Benbrik, D. Lemonnier, D. Blay, Laminar natural convection flow in a cylindrical cavity application to the storage of LNG, J. Petrol. Sci. Eng. 71 (2010) 126–132

[2] Z. Bocu, Z. Altac, Laminar natural convection heat transfer and air flow in three-dimensional rectangular enclosures with pin arrays attached to hot wall, Appl. Therm. Eng. 31 (2011) 3189–3195

[3] C. Sasmal, R.P. Chhabra, Effect of orientation on laminar natural convection from a heated square cylinder in power-law liquids, Int. J. Therm. Sci. 57 (2012) 112–125

[4] A. Chandra, R.P. Chhabra, Laminar free convection from a horizontal semi-circular cylinder to power-law fluids, Int. J. Heat Mass Transfer 55 (2012) 2934–2944

[5] A.K. Gupta, C. Sasmal, M. Sairamu, R.P. Chhabra, Laminar and steady free convection in power-law fluids from a heated spheroidal particle: a numerical study, Int. J. Heat Mass Transfer 75 (2014) 592–609

[6] D. Sadaoui, A. Sahi, H. Nadjib, B. Meziani, T. Amoura, Free convection in a square enclosure with a finned plate, Mech. Ind. 16 (2015) 310

[7] Y. Gulberg, Y. Feldman, On laminar natural convection inside multi-layered spherical shells, Int. J. Heat Mass Transfer 91 (2015) 908–921

[8] N.S. Gibanov, M.A. Sheremet, I. Pop, Free convection in a trapezoidal cavity filled with a micropolar fluid, Int. J. Heat Mass Transfer 99 (2016) 831–838

[9] C. Liao, C. Lin, Influences of a confined elliptic cylinder at different aspect ratios and inclinations on the laminar natural and mixed convection flows, Int. J. Heat Mass Transfer 55 (2012) 6638–6650

[10] M. Saidi, G. Karimi, Free convection cooling in modified L-shape enclosures using copperewater nanofluid, Energy 70 (2014) 251–271

[11] M. Bouhalleb, H. Abbassi, Natural convection of nanofluids in enclosures with low aspect ratios, Int. J. Hydrog. Energy 39 (2014) 15275–15286

[12] A. Sahi, D. Sadaoui, B. Meziani, K. Mansouri, Effects of thermal boundary conditions, surface radiation and aspect ratio on thermal performance in "T" shallow cavity, Mech. Ind. 15 (2014) 557–568

[13] S.C. Saha, Y.T. Gu, Natural convection in a triangular enclosure heated from below and non-uniformly cooled from top, Int. J. Heat Mass Transfer 80 (2015) 529–538

[14] S. Yigit, R.J. Poole, N. Chakraborty, Effects of aspect ratio on laminar Rayleigh–Bénard convection of power-law fluids in rectangular enclosures: a numerical investigation, Int. J. Heat Mass Transfer 91 (2015) 1292–1307

[15] S.M. Mirabedin, F. Farhadi, Natural convection in circular enclosures heated from below for various central angles, Case Stud. Therm. Eng. 8 (2016) 322–329

[16] D. Sadaoui, A. Sahi, A. Djerrada, K. Mansouri, Coupled radiation and natural convection within an inclined sinusoidal solar collector heated from below, Mech. Ind. 17 (2016) 302

[17] J. Baumgartl, A. Hubert, G. Muller, The use of magneto hydrodynamic effects to investigate fluid flow in electrically conducting melts, Phys. Fluids 5 (1993) 3280–3289

[18] J.S. Walker, B.F. Picologlou, G. Muller, Liquid metal flow in insulating rectangular expansion with a strong magnetic field, J. Fluid Mech. 305 (1995) 111–126

[19] R. Touihri, H. Ben Hadid, On the onset of convective instabilities in cylindrical cavities heated from below. II. Effect of a magnetic field, Phys. Fluids 11 (1998) 2089–2099

[20] P.A. Davidson, Magnetohydrodynamics in materials processing, Annu. Rev. Fluid Mech. 31 (1999) 273–300

[21] A. Juel, T. Mullin, H. Ben Hadid, D. Henry, Magnetohydrodynamic convection in molten gallium, J. Fluid Mech. 378 (1999) 97–118

[22] N.B. Morley, S. Smolentsev, L Barleon, I.R. Kirillov, M. Takahashi, Liquid magnetohydrodynamics – recent progress and future directions for fusion, Fusion Eng. Des. 51–52 (2000) 701–713

[23] P. Kandaswamy, S. Malliga Sundari, N. Nithyadev, Magneto-convection in an enclosure with partially active vertical walls, Int. J. Heat Mass Transfer 51 (2008) 1946–1954

[24] M. Pirmohammadi, M. Ghassemi, G.A. Sheikhzadeh, Effect of magnetic field on buoyancy driven convection in differentially heated square cavity, IEEE Trans. Magn. 45 (2009) 407–411

[25] M. Hasanuzzaman, H.F. Öztop, M.M. Rahman, N.A. Rahim, R. Saidur, Y. Varol, Magnetohydrodynamic natural convection in trapezoidal cavities, Int. Commun. Heat Mass Transfer 39 (2012) 1384–1394

[26] S.M. Aminossadati, B. Ghasemib, A. Kargar, Computational analysis of magnetohydrodynamic natural convection in a square cavity with a thin fin, Eur. J. Mech. B Fluids 46 (2014) 154–163

[27] B.K. Jha, B. Aina, S. Isa, Fully developed MHD natural convection flow in a vertical annular microchannel: an exact solution, J. King Saud Univ. Sci 27 (2015) 253–259

[28] M.M. Rahman, S. Mojumder, S. Saha, A.H. Joarder, R. Saidur, A.G. Naim, Numerical and statistical analysis on unsteady magnetohydrodynamic convection in a semi-circular enclosure filled with ferrofluid, Int. J. Heat Mass Transfer 89 (2015) 1316–1330

[29] A.K. Hussein, H.R. Ashorynejad, S. Sivasankaran, L. Kolsi, M. Shikholeslami, I.K. Adegun, Modeling of MHD natural convection in a square enclosure having an adiabatic square shaped body using Lattice Boltzmann Method, Alex. Eng. J. 55 (2016) 203–214

[30] N.M. Al-Najem, K.M. Khanafer, M.M. El-Refaee, Numerical study of laminar natural convection in tilted enclosure with transverse magnetic field, Int. J. Numer. Methods Heat Fluid Flow 8 (1998) 651–672

[31] M. Syou, T. Tagawa, H. Ozoe, Average heat transfer rates measured and numerically analyzed for combined convection of air in an inclined cylindrical enclosure due to both magnetic and gravitational fields, Exp. Therm. Fluid Sci. 27 (2003) 891–899

[32] M.C. Ece, E. Büyük, Natural-convection flow under a magnetic field in an inclined rectangular enclosure heated and cooled on adjacent walls, Fluid Dyn. Res. 38 (2006) 564–590

[33] M. Pirmohammadi, M. Ghassemi, Effect of magnetic field on convection heat transfer inside a tilted square enclosure, Int. Commun. Heat Mass Transfer 36 (2009) 776–780

[34] M.A. Teamah, A.F. Elsafty, E.Z. Massoud, Numerical simulation of double-diffusive natural convective flow in an inclined rectangular enclosure in the presence of magnetic field and heat source, Int. J. Therm. Sci. 52 (2012) 161–175

[35] S.H. Teamah, A.K. Hussein, R.N. Mohammed, Studying the effects of a longitudinal magnetic field and discrete isoflux heat source size on natural convection inside a tilted sinusoidal corrugated enclosure, Comput. Math. Appl. 64 (2012) 476–488

[36] N. Rudraiah, M. Venkatachalappa, C.K. Subbaraya, Combined surface tension and buoyancy-driven convection in rectangular open cavity the presence of a magnetic field, Int. J. Non-Linear Mech. 30 (1995) 759–770

[37] A.J. Chamkha, H. Al-Naser, Hydromagnetic double-diffusive convection in a rectangular enclosure with uniform side heat and mass fluxes and opposing temperature and concentration gradients, Int. J. Therm. Sci. 41 (2002) 936–948

[38] M. Changfeng, Lattice BGK simulations of double diffusive natural convection in a rectangular enclosure in the presences of magnetic field and heat source, Nonlinear Anal. Real World Appl. 10 (2009) 2666–2678

[39] M. Sathiyamoorthy, A. Chamkha, Effect of magnetic field on natural convection flow in a liquid gallium filled square cavity for linearly heated side wall(s), Int. J. Therm. Sci. 49 (2010) 1856–1865

[40] M. Venkatachalappa, Y. Do, M. Sankar, Effect of magnetic field on the heat and mass transfer in a vertical annulus, Int. J. Eng. Sci. 49 (2011) 262–278

[41] M.A. Mansour, M.A.Y. Bakier, Influence of thermal boundary conditions on MHD natural convection in square enclosure using Cu-water nanofluid, Energy Rep. 1 (2015) 134–144

[42] A.K. Hussein, M.A.Y. Bakier, M.B.B. Hamida, S. Sivasankaran, Magneto-hydrodynamic natural convection in an inclined T-shaped enclosure for different nanofluids and subjected to a uniform heat source, Alexandia, Eng. J. 55 (2016) 2157–2169

[43] M.A. Sheremet, I. Pop, N.C. Rosca, Magnetic field effect on the unsteady natural convection in a wavy-walled cavity filled with a nanofluid: Buongiorno's mathematical model, J. Taiwan Inst. Chem. Eng. 61 (2016) 211–222

[44] N.S. Bondareva, M.A. Sheremet, Effect of inclined magnetic field on natural convection melting in a square cavity with a local heat source, J. Magn. Magn. Mater. 419 (2016) 476–484
[45] C. Chen, C. Cheng, Predictions of buoyancy-induced flow in various across-shape concave enclosures, Int. Commun. Heat Mass Transfer 38 (2011) 442–448
[46] S.V. Patankar, Numerical Heat Transfer and Fluid Flow, Hemisphere Publishing Corporation, Taylor and Francis Group, New York, 1980, pp. 113–137
[47] I.E. Sarris, G.K. Zikos, A.P. Grecos, N.S. Vlachos, On the limits of validity of the low magnetic Reynolds number approximation in MHD natural-convection heat transfer, Numer. Heat Transf. B: Fundam. 50 (2006) 157–180

Cite this article as: A. Sahi, D. Sadaoui, N. Sadoun, A. Djerrada, Effects of magnetic field on natural convection heat transfer in a T-shaped cavity, Mechanics & Industry **18**, 407 (2017)